

8-15-1999

# Isotropic dielectric functions of highly disordered $\text{Al}_x\text{Ga}_{1-x}\text{InP}$ ( $0 \leq x \leq 1$ ) lattice matched to GaAs

Mathias Schubert

University of Nebraska - Lincoln, mschubert4@unl.edu

J. A. Woollam

University of Nebraska - Lincoln

G. Leibiger

Department of Semiconductor Physics, Faculty of Physics and Geoscience, University of Leipzig, D-04103 Leipzig, Germany

B. Rheinlander

Department of Semiconductor Physics, Faculty of Physics and Geoscience, University of Leipzig, D-04103 Leipzig, Germany

I. Pietzonka

University of Leipzig, Faculty of Chemistry and Mineralogy, Department of Solid State Chemistry, D-04103 Leipzig, Germany

See next page for additional authors

Follow this and additional works at: <http://digitalcommons.unl.edu/electricalengineeringfacpub>



Part of the [Electrical and Computer Engineering Commons](#)

---

Schubert, Mathias; Woollam, J. A.; Leibiger, G.; Rheinlander, B.; Pietzonka, I.; Sab, T.; and Gottschalch, V., "Isotropic dielectric functions of highly disordered  $\text{Al}_x\text{Ga}_{1-x}\text{InP}$  ( $0 \leq x \leq 1$ ) lattice matched to GaAs" (1999). *Faculty Publications from the Department of Electrical Engineering*. Paper 16.

<http://digitalcommons.unl.edu/electricalengineeringfacpub/16>

This Article is brought to you for free and open access by the Electrical Engineering, Department of at DigitalCommons@University of Nebraska - Lincoln. It has been accepted for inclusion in Faculty Publications from the Department of Electrical Engineering by an authorized administrator of DigitalCommons@University of Nebraska - Lincoln.

---

**Authors**

Mathias Schubert, J. A. Woollam, G. Leibiger, B. Rheinlander, I. Pietzonka, T. Sab, and V. Gottschalch

# Isotropic dielectric functions of highly disordered $\text{Al}_x\text{Ga}_{1-x}\text{InP}$ ( $0 \leq x \leq 1$ ) lattice matched to GaAs

M. Schubert<sup>a)</sup> and J. A. Woollam

*Center for Microelectronic and Optical Materials Research and Department of Electrical Engineering, University of Nebraska, Lincoln, Nebraska 68588*

G. Leibiger and B. Rheinländer

*Department of Semiconductor Physics, Faculty of Physics and Geoscience, University of Leipzig, D-04103 Leipzig, Germany*

I. Pietzonka, T. Saß, and V. Gottschalch

*University of Leipzig, Faculty of Chemistry and Mineralogy, Department of Solid State Chemistry, D-04103 Leipzig, Germany*

(Received 15 February 1999; accepted for publication 7 May 1999)

Determination of the complex dielectric function and the critical-point energies of  $(\text{Al}_x\text{Ga}_{1-x})_{0.51}\text{In}_{0.49}\text{P}$ , over the full range of composition  $x$  and for photon energies  $E$  from 0.75 to 5 eV is reported from variable angle of incidence spectroscopic ellipsometry. Native-oxide effects on the  $(\text{Al}_x\text{Ga}_{1-x})_{0.51}\text{In}_{0.49}\text{P}$  optical functions are removed numerically. The highly disordered state of the metalorganic vapor-phase epitaxy grown samples is analyzed by transmission electron microscopy. Optical anisotropy investigations revealed that the order-induced optical birefringence is negligible throughout. The augmentation of A. D. Rakić and M. L. Majewski [J. Appl. Phys. **80**, 5909 (1996)] to Adachi's critical-point model, i.e., consideration of Gaussian-like broadening function instead of Lorentzian broadening, is used for calculation of the isotropic  $(\text{Al}_x\text{Ga}_{1-x})_{0.51}\text{In}_{0.49}\text{P}$  dielectric function  $\epsilon$ . The optical functions spectra consistently match the experimental data, whereas previously reported model dielectric functions fail to reproduce the correct absorption behavior of the quaternary, especially near the fundamental band-to-band transition. The results are compared to those presented previously, and influence of spontaneous chemical ordering is discussed. © 1999 American Institute of Physics. [S0021-8979(99)04316-9]

## I. INTRODUCTION

Altering the composition of III–V semiconductor alloys allows tailoring of material properties such as band gap or refractive index in device structures for opto- and microelectronic applications.<sup>1</sup> The  $(\text{Al}_x\text{Ga}_{1-x})_{0.51}\text{In}_{0.49}\text{P}$  system lattice matched to GaAs (hereafter referred to as  $\text{Al}_x\text{Ga}_{1-x}\text{InP}$ ) is widely used in visible laser diodes as active layer or barrier material.<sup>2</sup> Today it is well known that the thermodynamics of the alloy system,<sup>1</sup> especially when grown by metalorganic vapor-phase epitaxy (MOVPE), produces material that may exhibit some degree of long-range chemical ordering. The state of ordering usually consists of the layered trigonal “Cu–Pt”-like structure, and is referred to as CuPt type (See, e.g., Fig. 1 in Ref. 3). The redshift  $\Delta E_0$  of the fundamental band-to-band transition energy  $E_0$  upon ordering is essential, and may amount to 430 meV for GaInP, or 270 meV for AlInP as recently calculated by Wei and Zunger.<sup>4</sup> Band-to-band transitions that involve higher photon energies  $E$  also split and shift as a function of ordering.<sup>5,6</sup> Band-to-band transitions involve critical points (CPs) in their joint density of states, and cause typical CP structures in the material dielectric function  $\epsilon$ .<sup>7</sup> As a consequence, chemical ordering alters dielectric function  $\epsilon = \epsilon_1 + i\epsilon_2$ , and optical function  $N = \sqrt{\epsilon} = n + ik$  of the alloy system, especially in the vicinity

of direct band-to-band transitions. Therefore, ignoring the state of chemical ordering of samples under investigation can lead to incorrect results. To obtain generally useful data for the quaternary system, such as optical functions spectra, knowledge of the state and the degree of ordering within a set of samples being investigated is essential. However, except for GaInP, quantifying the state of ordering in  $\text{Al}_x\text{Ga}_{1-x}\text{InP}$  remains a challenge yet today. Likewise, observance of perfect ordering, even for GaInP, is yet not reported. Nevertheless, highly disordered alloys may be grown at conditions that hinder or prevent the formation of chemical ordering.

Several spectroscopic studies of the  $\text{Al}_x\text{Ga}_{1-x}\text{InP}$  optical properties have been reported so far. Kato *et al.* investigated samples grown by MOVPE using spectroscopic ellipsometry (SE).<sup>8</sup> The authors report the compositional dependencies of the  $E_0$ ,  $E_1$ , and  $E_2$  CP-structure parameters. Kato *et al.* assumed that spontaneous ordering in  $\text{Al}_x\text{Ga}_{1-x}\text{InP}$  is impossible for  $x > 0$ . But today CuPt-type ordering is known to occur in  $\text{Al}_x\text{Ga}_{1-x}\text{InP}$  regardless of composition  $x$ .<sup>3,9,10</sup> According to the sample growth conditions and experimental data reported by Kato *et al.*, it is not unlikely that spontaneous ordering influenced their results. [Note, e.g., the redshift of the onset of absorption at the fundamental band edge for GaInP grown on (100)GaAs with 2°, 7°, and 15° miscuts (Fig. 1 in Ref. 8).] The authors further provide a model di-

<sup>a)</sup>Electronic mail: schubert@engrs.unl.edu

electric function (MDF)  $\epsilon(E, x)$  of the quaternary alloy for  $1.2 \text{ eV} \leq E \leq 5.5 \text{ eV}$ , and  $0 \leq x \leq 1$ . The MDF used by Kato *et al.* is Adachi's composite model that includes CP and damped-harmonic-oscillator (DHO) approximations.<sup>11,12</sup> This model provides wide spectral coverage but fails to reproduce  $\epsilon(E, x)$  near the fundamental band-to-band transition energy  $E_0$ , i.e., within the near-band-gap spectral range.<sup>13</sup> Below  $E_0$  the MDF clearly overestimates the imaginary, but underestimates the real part of  $\epsilon(E, x)$ . No attempt was made for numerical removal of native-oxide layer effects on  $\epsilon(E, x)$ .

Lee *et al.*<sup>14</sup> reported the composition dependencies of the  $E_1$ ,  $E_1 + \Delta_1$ , and  $E_2$  CP-structure parameters from SE investigations using the standard critical-point parabolic-band (CPPB) model.<sup>15,16</sup> The authors expected no CuPt-type ordering in their samples. A similar feature as that assigned by Lee *et al.* for the  $E_1 + \Delta_1$  transition was also observed by Alsina *et al.* on highly ordered samples.<sup>6</sup> Alsina *et al.* attributed this  $E_1$  CP splitting to the presence of CuPt ordering in their samples rather than splitting due to spin-orbit interaction in the valence bands of the disordered, and therefore zinc blende-type semiconductor alloys.<sup>6</sup> Wei, Franceschetti, and Zunger have shown theoretically that CuPt ordering splits the zinc blende-type  $E_1$  transition into at least three transitions. The amount of splitting should correlate with the band-gap reduction, and hence with the degree of ordering.<sup>5</sup> Alsina *et al.* indeed observed a linear dependence of the  $E_1$  splitting energy on the redshift of  $E_0$ . In our present work we have not observed the  $E_1$  splitting for highly disordered samples. It is possible that the structure assigned by Lee *et al.* as the  $E_1 + \Delta_1$  transition originated from a certain degree of chemical ordering within their samples. In a later work, Lee *et al.* studied the effect of CuPt-type ordering and doping in GaInP using SE and transmission electron microscopy (TEM).<sup>17</sup> The authors observe and explain shift and splitting of the  $E_1$  CP structure in relationship to the redshift of the fundamental band-to-band transition  $E_0$  by CuPt ordering. The authors find that carrier-related band-gap renormalization also affects the  $E_1$  CP structure. Raman and SE investigations of strain and disorder effects in  $\text{In}_x\text{Ga}_{1-x}\text{P}$  ( $0.25 \leq x \leq 0.8$ ) have also been studied by Lee *et al.*<sup>18</sup>

Adachi *et al.*<sup>19</sup> and Ozaki *et al.*<sup>20</sup> performed electroluminescence (ER), thermoreflectance (TR), and SE measurements at samples that, according to the growth conditions reported, may also obey spontaneous ordering. Adachi's composite model is employed for CP-parameter analysis. Adachi *et al.* and Ozaki *et al.* obtain composition dependencies for the  $E_0$ ,  $E_0 + \Delta_0$ ,  $E_1$ ,  $E_2$ , and  $E_2 + \delta$  CP parameters.<sup>19,20</sup> Prior to these reports, Adachi *et al.* determined refractive indices in the 1.2–2.9 eV photon-energy range.<sup>21</sup> Ozaki *et al.*<sup>20</sup> provide model parameters for  $\epsilon(E, x)$  at  $x = 0, 0.25, 0.5, 0.75$ , and 1. But, similar to  $\epsilon(E, x)$  given by Kato *et al.*, the imaginary part of  $\epsilon(E, x)$  given by Ozaki *et al.* is clearly overestimated within the near-band-gap spectral range, and does not vanish within the band gap. Therefore, the MDFs provided by Kato *et al.* and Ozaki *et al.* are not generally useful for modeling multiple-layer structures, especially within the near-band-gap spectral range.

TABLE I. Sample parameters for the  $\text{Al}_x\text{Ga}_{1-x}\text{InP}$  layers grown at 720 °C by MOVPE on (001)GaAs with 6° miscut toward the nearest (111)Ga plane.

$x$	0	0.33	0.48	0.7	0.82	1
$f_{\text{V/III}}$	555	282	334	542	511	253
$\left(\frac{\Delta a}{a}\right)_\perp 10^{-4}$	-10	3	16	2	-5	-4
$d$ [nm]	801	951	1224	262	413	913
$d_z$ [nm]	4	4	4	5	3	7

Moser *et al.*<sup>22</sup> have investigated  $\text{Al}_x\text{Ga}_{1-x}\text{InP}$  samples obtained at various growth conditions, and with compositions  $x = 0, 0.33$ , and 0.66. The authors report a parameterization of the quaternary refractive index values  $n(E, x)$  for  $x \leq 0.66$ , and for photon energies  $E$  between the reststrahlen band and the fundamental band-gap energy  $E_0$ . Except for the shift of the absorption edge, the authors find no appreciable changes of the refractive indices between ordered and disordered samples.

The purpose of the present work is to provide more accurate dielectric functions data for the  $\text{Al}_x\text{Ga}_{1-x}\text{InP}$  system. The intention is further to provide data on a sample set with a known state of chemical ordering. Therefore, an attempt is made to *avoid* chemical ordering. Samples are intentionally grown at temperatures and substrate miscuts that hinder the formation of ordering during the epitaxial growth.<sup>1</sup> TEM and optical anisotropy investigations are used to confirm the state of ordering. The samples investigated show very little or no ordering related effects, such as the additional superlattice diffraction spots,<sup>23</sup> or the ordering-induced birefringence centered at the fundamental band-to-band transition  $E_0$ .<sup>9,24</sup> Adachi's dielectric function model is employed for calculation of  $\epsilon(x, E)$ . Rakić and Majewski<sup>13</sup> recently augmented this optical dielectric function model by introducing Gaussian-like broadening instead of Lorentzian broadening. In the present article, Gaussian-like broadening is considered as well, and model parameters are provided for  $\epsilon(x, E)$  with wide spectral coverage, and for improved accuracy within the near-band-gap spectral range. The dielectric functions and CP-structure parameters obtained here are compared to those from other authors.

## II. EXPERIMENT

The  $(\text{Al}_x\text{Ga}_{1-x})\text{InP}$  samples were grown by MOVPE at a growth temperature of 720 °C on (001)GaAs with 6° miscut towards the nearest (111)Ga plane. All epitaxial layers were intentionally undoped. The high growth temperature and the substrate miscut toward the (111)Ga plane hindered the formation of spontaneous ordering during growth.<sup>1</sup> Prior to the epilayer growth, a GaAs-buffer layer of about 300 nm thickness was deposited. The investigated compositions are  $x = 0, 0.33, 0.48, 0.7, 0.82$ , and 1. The thickness of the epilayers ranges from 262 to 1224 nm (Table I). The perpendicular lattice mismatch  $\Delta a/a_\perp$  of the epilayer to the GaAs substrate was measured by double-crystal x-ray diffraction using the (004) reflex of both the substrate and the epilayer.

All samples were measured at room temperature by variable-angle spectroscopic ellipsometry (VASE) at photon

energies  $E$  from 0.75 to 5.0 eV. The rotating-analyzer ellipsometer is equipped with an automated compensator function that allows accurate determination of the ellipsometric parameter  $\Delta$  within the full range from  $0^\circ$  to  $360^\circ$ , and a 75 W Xenon lamp as light source. The measurements were carried out at multiple angles of incidence ( $70^\circ$ ,  $74^\circ$ , and  $78^\circ$ ).

Prior to VASE measurements the samples were investigated by TEM to confirm their highly disordered state. Selected area diffraction patterns did not or only minimally reveal the well-known additional spots due to the alternating sublattice planes of CuPt-ordered compounds.<sup>23</sup> We also performed optical anisotropy investigations on all samples. CuPt-ordering redshifts and splits the band-gap and valence band states at the center of the Brillouin zone, respectively. It was shown previously that the splitting of the valence band is accompanied by a strong dichroism centered at the fundamental band-to-band transition.<sup>10,24</sup> This birefringence can be used to estimate the relative degree of ordering  $\eta$  regardless of the composition  $x$ . (The degree of ordering  $\eta$  is defined as the difference between the alloy compositions of two subsequent sublattice planes within the CuPt superlattice.<sup>3</sup>) The cross-polarized optical transmission spectrum of a CuPt-ordered  $\text{Al}_x\text{Ga}_{1-x}\text{InP}$  thin film, after wet-chemical removal of the substrate material, reveals sharp bands near  $E_0$ . The line shape of the cross-polarized transmission spectrum depends on the ordered state within the epitaxial layer. This technique is called “dark-field spectroscopy” (DFS),<sup>10,24</sup> and was used for sample selection. We have extended our birefringence investigations to the  $\text{Al}_x\text{Ga}_{1-x}\text{InP}$  system, and we find that regardless of the composition  $x$  CuPt-ordering induces the same birefringence near  $E_0$  as in GaInP or AlInP.<sup>25</sup> Samples with composition  $x=0$  and  $x=1$  revealed no DFS signal and are disordered. The quaternary samples are at least highly disordered, and we estimate that these samples have less than about 10% ordering, i.e.,  $\eta \leq 0.1$ .

### III. THEORY

Ellipsometry can determine the dielectric function  $\epsilon$  and thickness  $d$  of a thin-film sample by comparing the measured data with a model calculation. The standard ellipsometric parameters are defined through  $\Psi$  and  $\Delta$ . They are related to the complex reflectance ratio  $\rho$

$$\rho \equiv \frac{r_p}{r_s} = \tan \Psi \exp i\Delta, \quad (1)$$

where  $r_p$ , and  $r_s$  are the reflection coefficients for light polarized parallel ( $p$ ) and perpendicular ( $s$ ) to the plane of incidence, respectively.<sup>26</sup> The pseudodielectric function  $\langle \epsilon \rangle$  is a common representation of the ellipsometric data  $\Psi$  and  $\Delta$  via the two-phase (ambient-substrate) model<sup>26</sup>

$$\langle \epsilon \rangle = \epsilon_a [(1 - \rho)/(1 + \rho)]^2 \sin^2 \Phi_a + \cos^2 \Phi_a \tan^2 \Phi_a. \quad (2)$$

The ambient dielectric function  $\epsilon_a$  is unity. The ellipsometric parameters depend on the photon energy  $E$ , the sample layer structure, the material dielectric function, and the angle of incidence  $\Phi_a$ . A model calculation is needed for sample analysis.<sup>27</sup> We use a two-layer model that accounts for the substrate, the  $\text{Al}_x\text{Ga}_{1-x}\text{InP}$  layer, the native-oxide layer, and

the ambient. The model calculation employs well-known algebraic matrix approaches, and relates the ellipsometric parameters to the dielectric functions and thickness of the thin-film sample.<sup>26,27</sup> Tabulated data are used for the substrate dielectric function values. The dielectric function and thickness of both the  $\text{Al}_x\text{Ga}_{1-x}\text{InP}$  layer and the native-oxide layer remain as unknown parameters. The number of unknown parameters for data analysis can be reduced if appropriate MDFs for the materials of interest are available. A regression analysis is then used to vary the model parameters until the calculated  $(\Psi_{ij}^c, \Delta_{ij}^c)$ , and measured data  $(\Psi_{ij}, \Delta_{ij})$  match as closely as possible. This is done by minimizing the mean square error ( $\chi^2$ ) function which is weighted to the estimated experimental errors  $(\sigma_{ij}^\Psi, \sigma_{ij}^\Delta)$ <sup>28</sup>

$$\chi^2 = \frac{1}{2MN} \sum_{i,j} \left[ \left( \frac{\Psi_{ij} - \Psi_{ij}^c}{\sigma_{ij}^\Psi} \right)^2 + \left( \frac{\Delta_{ij} - \Delta_{ij}^c}{\sigma_{ij}^\Delta} \right)^2 \right]. \quad (3)$$

The indices  $i$  and  $j$  indicate data sets  $(\Psi, \Delta)$  at photon energy  $E_i$ , and angle of incidence  $\Phi_{aj}$ . For ellipsometric data analysis simple parametric optical functions such as the Cauchy model for dielectrics,<sup>27</sup> or the Zollner model for semiconductor native oxides<sup>29</sup> are often utilized.<sup>30</sup> General parametric models, i.e., MDFs that completely describe CP structure and line shape of the dielectric function of semiconductors, are complex, and have been developed, e.g., by Kim *et al.*<sup>31</sup> and Kim, Garland, and Raccach.<sup>32</sup> Such models reveal information about CP energy, CP broadening, and the joint density of states. Accurate CP energies and linewidths are then obtained from analysis of ellipsometric data and their derivatives.<sup>32,33</sup>

We employ Adachi's critical-point composite model for parametrization of the  $\text{Al}_x\text{Ga}_{1-x}\text{InP}$  dielectric function  $\epsilon(x, E)$ .<sup>11,12</sup> Adachi's MDF is based on the one-electron interband-transition approach, and includes terms for the  $E_0$ ,  $E_0 + \Delta_0$ ,  $E_1$ , and  $E_1 + \Delta_1$  transitions, and phenomenological terms that describe contributions from higher-lying direct transitions. Application of the MDF for analysis of  $\epsilon$  from a large variety of compound semiconductors has been reported by numerous authors. We omit a detailed introduction to the Adachi MDF, and the reader is referred to, e.g., Refs. 8, 11, 12, 13, 19, 20, and references therein. (The complete set of equations for the MDF used here is given in the Appendix of the present work.) Instead, we briefly outline the augmentation of Adachi's MDF by Gaussian-like broadening functions suggested recently by Rakić and Majewski.<sup>13</sup>

Adachi's MDF includes damped harmonic oscillator (DHO) functions to model the strong maximum in  $\epsilon_2$  known for many III-V compounds as the  $E_2$  peak. This structure contains contributions from numerous transitions within the Brillouin zone.<sup>7</sup> Two other weak transitions labeled  $E'_0$  and  $E'_1$  superimpose the  $E_2$  peak.<sup>15</sup> The DHO approximation well reproduces experimental data within the region of the  $E_2$  peak, but introduces considerable absorption below the band gap. Likewise, a damped Lorentzian (DL) function accounts for the excitonic contributions to the  $E_1$  CP structure. But the imaginary part of this line shape also yields physically unreasonable absorption for photon energies less than the fundamental gap energy  $E_0$ . The total



below-gap absorption introduced by the DL and DHO functions is a shortcoming of Adachi's composite model. Kim *et al.*,<sup>31,32</sup> and Rakić and Majewski<sup>13</sup> demonstrated that the high absorption below the band gap introduced by the higher-lying CPs is due to inappropriate linewidth approximation which results in Lorentzian broadening. Kim *et al.* proposed a model which is superior in accuracy to that of Adachi but also very complex.<sup>31,32</sup> This model accounts for the analytic form of the joint density of states and allows for Gaussian broadening. Instead, Rakić and Majewski suggest to replace each energy-independent broadening constants  $\Gamma$  in Adachi's composite model by Gaussian-like energy-dependent broadening functions<sup>13</sup>

$$\tilde{\Gamma} = \Gamma \exp[-s(E - E_i)^2] \quad (4)$$

introducing the value  $s$  as an additional parameter. Except for photon energies  $E$  near the resonance  $E_i$  the energy-dependent broadening effectively reduces  $\epsilon_2$ . The parameter  $s$  adjusts the line shape of the broadening function  $\tilde{\Gamma}$  continuously from that of a Lorentzian ( $\alpha = s\Gamma^2 = 0$ ) to a Gaussian ( $\alpha = s\Gamma^2 = 0.30$ ; see Fig. 1 in Ref. 13.). Hence, a broad range of broadening functions can be modeled. Rakić and Majewski successfully applied their extension for calculation of accurate GaAs and AlAs optical dielectric functions.<sup>13</sup> In particular, the authors could eliminate the incorrect absorption in the  $E_0$  CP region inherent to the Adachi model with Lorentzian broadening.

In this work we follow the approach used in Ref. 13 and employ Gaussian-like broadening functions within Adachi's MDF. Sufficient accuracy of the line shape fit was obtained after changing the broadening dependencies of the DL and DHO functions only. Second, we allow complex amplitudes for both DL and DHO functions, i.e., we replace  $A_i \rightarrow A_i \exp(ip_i)$  for the exciton contribution at the  $E_1$  CP structure ( $A_{1x}, p_{1x}$ ), and for the  $E_2$  CP term ( $A_2, p_2$ ). The exponential phases  $p_i$  cause asymmetry in both the DL and DHO functions, and primarily improve the fit quality. A complex amplitude may account somewhat for the fact that both CP structures actually contain many transitions. However, we prefer to treat the  $p_i$  as additional line shape parameters. Moreover, in the strict sense, the Gaussian-like broadening and the complex amplitudes violate the Kramers–Krönig (KK) consistency of Eqs. (A3) and (A4) (see Appendix), especially for large parameters  $s$  and  $p$ . Users of the present model should be aware of this inconsistency, and numerical KK transformation of the resulting model dielectric function is necessary. We checked the KK consistency of  $\epsilon(x, E)$  obtained in this work. Except for a constant offset due to high-energy contributions to the imaginary part not directly included here, we only find deviations less than the experimental error bars.

For  $\text{Al}_x\text{Ga}_{1-x}\text{InP}$  we include contributions to  $\epsilon(x, E)$  for each of the  $E_0(\in^{(0)})$ ,  $E_1(\in^{(1)})$ , and  $E_2(\in^{(2)})$  CP structure. The  $E_1$  CP structure further contains an excitonic term ( $\in^{(1x)}$ )

$$\epsilon = \epsilon_\infty + \epsilon^{(0)} + \epsilon^{(1)} + \epsilon^{(1x)} + \epsilon^{(2)}. \quad (5)$$

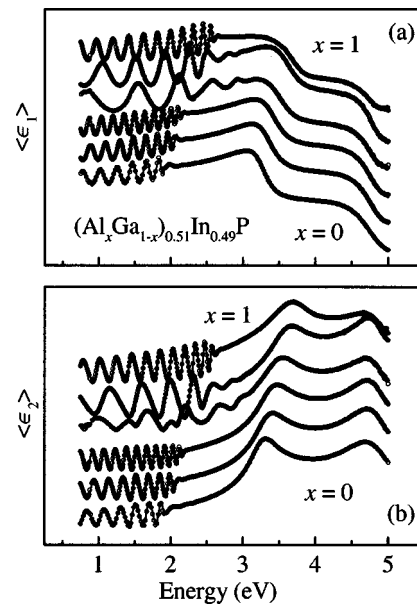


FIG. 1. Pseudodielectric function  $\langle \epsilon \rangle = \langle \epsilon_1 \rangle + i\langle \epsilon_2 \rangle$  of highly disordered  $\text{Al}_x\text{Ga}_{1-x}\text{InP}$  ( $x = 0, 0.3, 0.48, 0.7, 0.82, 1$ ). The solid lines correspond to the best fit ( $\chi^2 = 0.185$ ) of the experimental data (symbols) to the  $\text{Al}_x\text{Ga}_{1-x}\text{InP}$  model dielectric function parameters and layer thickness by simultaneous analysis of all compositions, and with numerical oxide-layer removal. Graphs are shifted for convenience. [ $\langle \epsilon_1 \rangle$ : (a),  $\langle \epsilon_2 \rangle$ : (b)].

The “static” dielectric constant  $\epsilon_\infty$  accommodates contributions from CP structures at high-energy transitions not directly included in this model. A second-order composition dependence for all individual parameters  $y$  of the MDF is assumed, i.e.,  $y = a_0 + xa_1 + x(1-x)b$ . Note that contributions due to spin-orbit interactions are omitted because the  $E_0 + \Delta_0$  and  $E_1 + \Delta_1$  transitions are not detected. The functions  $\in^{(0)}$ ,  $\in^{(1)}$ ,  $\in^{(1x)}$ , and  $\in^{(2)}$  are given in the Appendix below.

For treatment of the native-oxide layer present on all samples investigated we follow the Zollner approach, and employ the following model for the oxide dielectric function (ODF).<sup>29</sup>

$$\epsilon(E) = c + A[E^2 - E_z^2 - iE\Gamma_z \exp(-s_z[E - E_z]^2)]^{-1}. \quad (6)$$

#### IV. RESULTS AND DISCUSSIONS

Figure 1 shows real (a) and imaginary (b) parts of the pseudodielectric function  $\langle \epsilon \rangle$  obtained from the  $\text{Al}_x\text{Ga}_{1-x}\text{InP}$  samples investigated in this work. The graphs are shifted for convenience with increasing Al-composition  $x$ . The symbols refer to the experimental VASE data, and the solid lines correspond to the best-fit calculation (The total of the error function  $\chi^2$  that includes all data sets was 0.185). Near and below the band-gap energy  $E_0$  the  $\langle \epsilon \rangle$  spectra are dominated by multiple reflections within the film interfaces, and different interference patterns belong to different thicknesses of the  $\text{Al}_x\text{Ga}_{1-x}\text{InP}$  layer  $d$  (Table I). Note that the best-fit calculation accurately matches the experimental data, especially within the near-band-gap spectral range.

The experimental data were analyzed using a multiple-sample best-fit procedure. This approach employs the simultaneous minimization of all weighted error functions  $\chi^2$  for

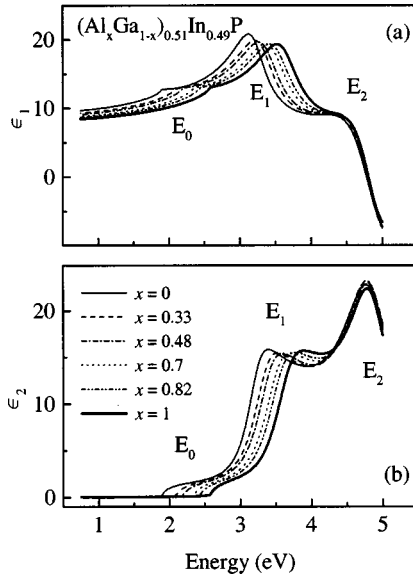


FIG. 2. Dielectric function  $\epsilon = \epsilon_1 + i\epsilon_2$  of highly disordered  $\text{Al}_x\text{Ga}_{1-x}\text{InP}$  extracted from the multiple-sample analysis. [ $\epsilon_1$ : (a),  $\epsilon_2$ : (b)].

each experimental data set, and the respective model calculation, where all model calculations share a common set of parameters. This set of parameters consists of the compositional dependencies  $a_0$ ,  $a_1$ , and  $b$  for each  $\text{Al}_x\text{Ga}_{1-x}\text{InP}$  MDF parameter  $y$ , the  $\text{Al}_x\text{Ga}_{1-x}\text{InP}$ -layer thickness  $d$ , and the oxide-layer thickness  $d_z$  for each sample, and the ODF parameters ( $c, A, E_z, \Gamma_z, s_z$ ). Each model calculation was based on a two-layer model. Tabulated data are used for the GaAs dielectric function. The second layer is included to account for the native-oxide layer known to cover most of semiconductor surfaces after exposure to normal conditions. Numerical data for the native-oxide dielectric function for  $\text{Al}_x\text{Ga}_{1-x}\text{InP}$  alloys are not available. Recently, Zollner reported ODF data for GaP and InP, and the dielectric functions spectra are not too different from each other.<sup>29</sup> A common set of oxide optical data is assumed for all samples, i.e., the  $\text{Al}_x\text{Ga}_{1-x}\text{InP}$  ODF is treated independently of  $x$ . The best-fit ODF parameters for the  $\text{Al}_x\text{Ga}_{1-x}\text{InP}$  native oxide are  $c = 1.76$ ,  $A = 7.45 \text{ eV}^{-2}$ ,  $E_z = 5.3 \text{ eV}$ ,  $\Gamma_z = 4.89 \text{ eV}$ , and  $s = 0.3 \text{ eV}^{-2}$ .

Figures 2 and 3 show the best-fit  $\text{Al}_x\text{Ga}_{1-x}\text{InP}$  optical functions spectra in terms of  $\epsilon(E, x)$  [Figs. 2(a) and 2(b)], or  $N(E, x)$  [Figs. 3(a) and 3(b)]. Table II lists the  $\text{Al}_x\text{Ga}_{1-x}\text{InP}$  MDF parameters. A smooth composition dependence for the optical functions spectra is obtained. We performed numerical KK transformation for each composition investigated, and we find KK consistency of  $\epsilon(E, x)$  within the experimental error bars. We note, however, that the individual contributions  $\epsilon^{(1x)}$  and  $\epsilon^{(2)}$  do not fully satisfy the KK requirement.

Below the band-gap  $E_0$  the refractive index values decrease with increasing Al-concentration  $x$ . The  $E_0$ ,  $E_1$ , and  $E_2$  CP structures are clearly resolved for all samples investigated. The band-to-band transitions  $E_0$  and  $E_1$  shift toward higher photon energies with increasing Al-concentration  $x$ , whereas the  $E_2$  peak remains almost unchanged. The bowing parameter  $b$  is negative, and of similar magnitude for the  $E_0$

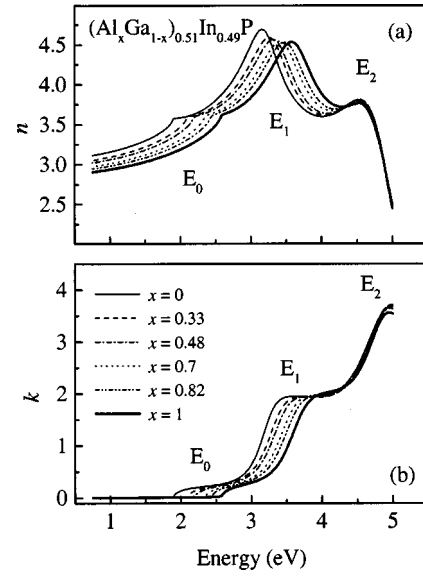


FIG. 3. Same as Fig. 2 for  $N = n + ik$  [ $n$ : (a);  $k$ : (b)].

and  $E_1$  CP energies. The  $E_0$  and  $E_1$  transition energies increase by 683 and 421 meV, respectively, whereas the  $E_2$ -peak energies of  $\text{AlInP}$  and  $\text{GaInP}$  are effectively the same. (The quantity  $a_1$  in Table II is the maximum change of a MDF parameter between  $\text{GaInP}$  [ $x=0$ ], and  $\text{AlInP}$  [ $x=1$ ]). The composition dependencies of the  $E_0$ ,  $E_1$ , and  $E_2$  transitions are (The estimated uncertainty for each parameter is less than or equal to 2% for 95% reliability.)

$$E_0[\text{eV}] = 1.899 + 0.683x - 0.12x(1-x) \{\pm 2\% \}, \quad (7)$$

$$E_1[\text{eV}] = 3.224 + 0.421x - 0.13x(1-x) \{\pm 2\% \}, \quad (8)$$

$$E_2[\text{eV}] = 4.832 - 0.02x \{\pm 2\% \}. \quad (9)$$

Figure 4 contains the individual CP contributions to the  $\text{Al}_x\text{Ga}_{1-x}\text{InP}$  MDF. The  $E_1$  CP structure shown here consists of both the one-electron term [Eq. (A2)], and the excitonic term [Eq. (A3)] in the Appendix. The amplitude of the

TABLE II. Best-fit results for the MDF parameters of highly disordered  $\text{Al}_x\text{Ga}_{1-x}\text{InP}$ .

CP contribution	Parameter $y = a_0 + xa_1 + x(1-x)b$			
	$y$	$a_0$	$a_1$	$b$
$\epsilon^{(0)}$	$\epsilon_\infty$	0.52	-0.08	-0.17
	$E_0$ (eV)	1.899	0.683	-0.12
	$A_0$ ( $\text{eV}^{1.5}$ )	10.44	11.34	-0.47
	$\Gamma_0$ (eV)	0.003	0.005	0.05
$\epsilon^{(1)}$	$E_1$ (eV)	3.224	0.421	-0.13
	$A_1$	5.27	-0.64	-1
$\epsilon^{(1x)}$	$\Gamma_1$ (eV)	0.334	0	0.32
	$A_{1x}$ (eV)	1.79	0.07	1.46
	$\Gamma_{1x}$ (eV)	0.295	0.046	-0.09
	$s_{1x}$ ( $\text{eV}^{-2}$ )	0.42	0.6	0
	$p_{1x}$	-0.76	0	0
$\epsilon^{(2)}$	$E_2$ (eV)	4.832	0.02	0
	$A_2$	2.19	-0.68	0.66
	$\Gamma_2$ (eV)	0.743	-0.159	0.05
	$s_2$ ( $\text{eV}^{-2}$ )	0.88	0.49	0
	$p_2$	0.16	0.1	-0.1

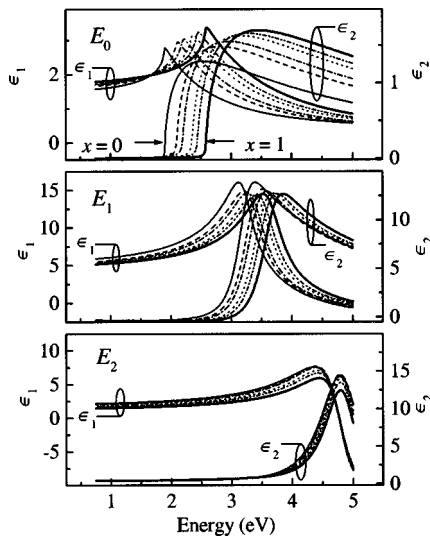


FIG. 4. Individual critical-point contributions to the  $\text{Al}_x\text{Ga}_{1-x}\text{InP}$  model dielectric function. The  $E_1$  CP structure consists of a 2D- $M_0$  CP, and a 2D-exciton contribution [Eqs. (A2) and (A3) in the Appendix]. The parameters used for calculation are given in Table II.

$E_1$  CP-structure  $A_1$  decreases with slight negative bowing from GaInP to AlInP. Note that Kato *et al.* found a similar decrease in  $A_1$  but with positive bowing.<sup>8</sup> Note further that the imaginary parts of the  $E_1$  and  $E_2$  CP structures vanish accordingly below the band gap  $E_0$ . The additional parameters  $s_{1x}$  and  $s_2$  for the broadening dependence of the DL and DHO functions depend on  $x$ , and are similar to those obtained by Rakić and Majewski for AlAs ( $\alpha_{1x}=0.01$ ,  $\alpha_2=0.27$ ) and GaAs ( $\alpha_{1x}=0.01$ ,  $\alpha_2=0.06$ ).<sup>13</sup> For GaInP (AlInP), e.g., it follows from  $s_{1x}=0.245 \text{ eV}^{-2}$  ( $1.02 \text{ eV}^{-2}$ ) and  $\Gamma_{1x}=0.245 \text{ eV}$  (0.291 eV) that  $\alpha_{1x}=s_{1x}\Gamma_{1x}^2=0.02$  (0.08), and from  $s_2=0.88 \text{ eV}^{-2}$  ( $1.37 \text{ eV}^{-2}$ ) and  $\Gamma_2=0.743 \text{ eV}$  (0.584 eV) that  $\alpha_2=s_2\Gamma_2^2=0.49$  (0.47), respectively.

Figure 5 shows the compositional dependencies of the  $E_0$  and  $E_1$  transition energies (squares and solid lines) in comparison with those obtained by Kato *et al.* (circles and dotted line),<sup>8</sup> Lee *et al.* (up triangles and short-dashed line,  $E_1$  transition energy only),<sup>14</sup> Ozaki *et al.* (down triangles and dash-dotted line),<sup>20</sup> and Adachi *et al.* (diamonds and dashed line).<sup>19</sup> The symbols belong to the actual compositions investigated, the lines are the composition dependencies (linear or second-order best-fit) as reported by the authors. General agreement of the  $E_0$ -CP energy dependencies reported so far with that obtained here is observed, and data are nearest to those from Adachi *et al.* This implies that, at least for most of the samples investigated, chemical ordering did not significantly influence previously reported dielectric function data. A small bowing parameter is found here in agreement with Adachi *et al.*, whereas no bowing was observed by Kato *et al.* It is possible that the small bowing parameter obtained here is related to the small degree of CuPt ordering of the quaternary samples. Yet the linear composition dependence of  $E_0$  assumed by Kato *et al.* slightly underestimates the lowest direct band-to-band transition energy of AlInP. The present GaInP  $E_0$  value is in excellent agreement with the

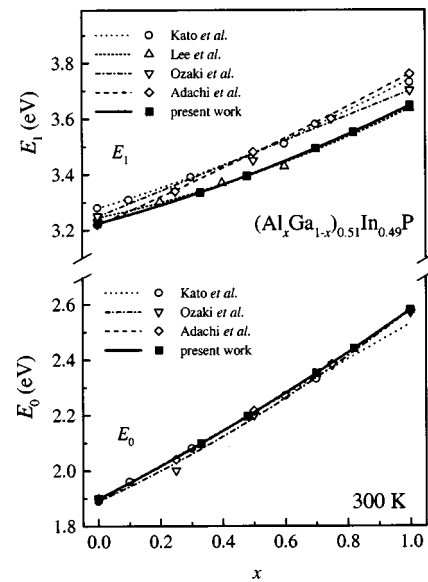


FIG. 5. Critical-point energies  $E_0$  and  $E_1$  of highly disordered  $\text{Al}_x\text{Ga}_{1-x}\text{InP}$  at room temperature [circles and dotted lines: Kato *et al.*, up triangles and short-dashed line: Lee *et al.* ( $E_1$  only), down triangles and dash-dotted lines: Ozaki *et al.*, diamonds and dashed lines: Adachi *et al.*, squares and solid lines: present study].

room-temperature band-gap energy of 1.9 eV measured previously for the disordered alloy.<sup>34</sup> (Note that the results in Ref. 35 obtained recently for GaInP from SE investigations indeed were influenced by spontaneous ordering within the group of samples investigated there. The  $E_0$  value of 1.87 eV there indicates the redshift of the fundamental gap due to CuPt ordering.)

The compositional dependence for the  $E_1$  energy is nearly identical to that presented by Lee *et al.*<sup>14,17</sup> (Note that the GaInP  $E_1$  value of 3.241 eV in Ref. 17 is closer to our value of 3.224 eV than the 3.245 eV obtained in Ref. 14.) The CP data reported by Adachi *et al.* coincide with our results for GaInP only. The latter is noticeable because we find the same  $E_0$  value but a different  $E_1$  value for AlInP than Adachi *et al.* The composition dependence for the  $E_1$  energy reported by Kato *et al.*, Ozaki *et al.*, and Adachi *et al.* by SE, TR, and ER, respectively, seem to agree well with each other, but are consistently shifted to higher energies with respect to the present results and those of Lee *et al.* Note further that only the reports of Lee *et al.* and the present work employed a second-derivative analysis of the ellipsometric data. Also, Lee *et al.* used the CPPB model for line shape analysis instead of Adachi's MDF. The apparent systematic difference between the  $E_1$  composition dependencies obtained either by best-fit analysis with numerical differentiation of experimental SE data or best-fit analysis of SE and modulation spectra is possibly due to the different model approaches used. The CP energies obtained here using Adachi's composite model with Gaussian-like broadening match those using the CPPB model rather than those derived from line shape analysis using Adachi's model with Lorentzian broadening.

As mentioned above, spin-split-related transitions are not detected within the present experimental data. The



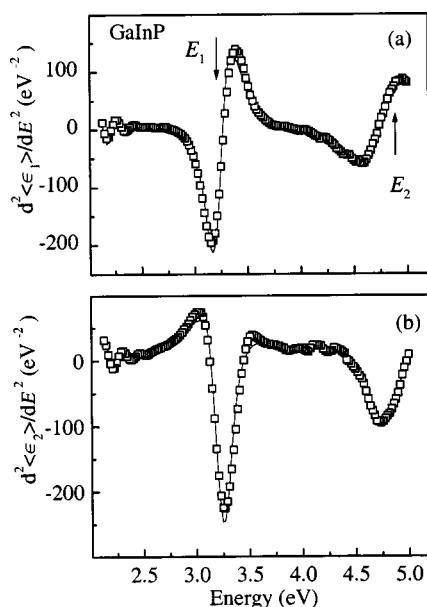


FIG. 6. Second derivative of the real [ $\langle\epsilon_1\rangle$ : (a)], and imaginary part [ $\langle\epsilon_2\rangle$ : (b)] of the pseudodielectric function ( $\epsilon$ ) of disordered GaInP (symbols: experimental data; solid lines: best fit).

second-derivative spectra of the ellipsometric parameters are usually very sensitive to CP structures of semiconductor alloys.<sup>31,32,33</sup> Figure 6 demonstrates that no other CP structures than the  $E_0$ ,  $E_1$ , and  $E_2$  transitions are resolved from the data. The pseudodielectric function spectra of the GaInP sample is used for presentation of a second-derivative line shape for a disordered sample. The numerical derivative of  $\langle\epsilon\rangle$  is obtained by locally fitting a polynomial to the ellipsometric data.<sup>36</sup> The second-degree fitting polynomial is obtained using 21 data points centered at the spectral position of interest, and the data step size is 5 meV. Except for their spectral position, the features shown in Fig. 6 are independent of the composition  $x$ , i.e., the data shown are typical for all samples. In particular, neither the  $E_0 + \Delta_0$  nor the  $E_1 + \Delta_1$  transition is resolved here for any of the samples. The observation of the  $E_1 + \Delta_1$  transition in disordered GaInP by Lee *et al.* mainly results from line shape fit of the pseudodielectric function spectra, and the  $E_1 + \Delta_1$  transition within the SE data presented there is actually difficult to recognize (e.g., Fig. 2 in Ref. 17).

Figure 7 compares optical constant data within the near-band-gap spectral range (solid lines) for  $x=0, 0.5$ , and 1 with those obtained by Moser *et al.* (symbols),<sup>22</sup> Kato *et al.* (dotted lines),<sup>8</sup> and Ozaki *et al.* (dash-dotted lines).<sup>20</sup> Moser *et al.* report refractive index values for compositions  $x \leq 0.66$ , and for photon energies  $E < E_0$ . Note excellent agreement between the refractive index value of Moser *et al.* and those obtained in this work. Note further that, except for photon energies near the band gap, the GaInP refractive index values are consistent with those obtained previously for a group of GaInP samples which were influenced by spontaneous CuPt-type ordering.<sup>35</sup> This finding is in agreement with previous observations for GaInP reported by Moser *et al.*<sup>22</sup> We also note good agreement between the real part of the  $\text{Al}_x\text{Ga}_{1-x}\text{InP}$  MDF and that presented by Ozaki *et al.* As

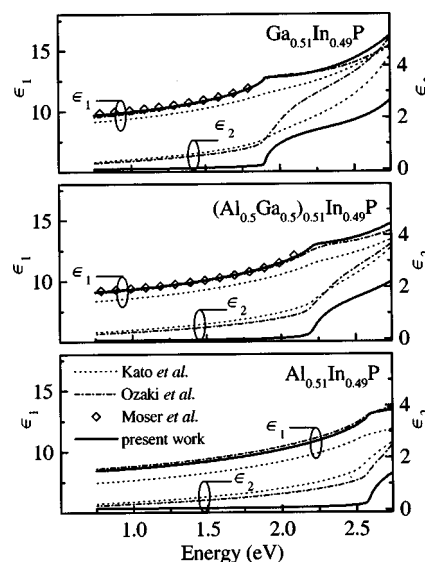


FIG. 7. Near-band-gap dielectric functions data [ $\epsilon(E,x)$ ;  $x=0, 0.5, 1$ ] for  $\text{Al}_x\text{Ga}_{1-x}\text{InP}$  (solid lines). The below-gap refractive index values reported by Moser *et al.* for  $x=0$  and  $x=0.5$  are shown for comparison (symbols). The MDF data presented by Kato *et al.* (dotted lines), and Ozaki *et al.* (dash-dotted lines), overestimate the imaginary part of  $\epsilon(E,x)$  within the band gap. The MDF given by Kato *et al.* also underestimates the real part of  $\epsilon(E,x)$ , and provides too small refractive index values.

mentioned in Sec. I, the imaginary part of the MDF provided by Ozaki *et al.*, however, yields physically unreasonable values below the band-gap  $E_0$ . The MDF reported by Kato *et al.* results in refractive index values that are not consistent with those reported by Moser *et al.*, Ozaki *et al.*, and the data reported in this work. It is likely that the real part of the MDF presented by Kato *et al.* is underestimated. Also, similar to the MDF given by Ozaki *et al.*, the imaginary part within the band gap given by Kato *et al.* is overestimated.

Besides shifting and splitting of CP structures, CuPt-type ordering also causes anisotropy of the dielectric function. Birefringence effects such as dependence of spectroscopic ellipsometry or reflectance difference data on the sample azimuth orientation have been reported for highly ordered samples by Alsina *et al.*,<sup>37</sup> Lee *et al.*,<sup>17</sup> and Luo *et al.*<sup>38,39</sup> However, Wirth *et al.* find that the ordering induced birefringence below the band-gap  $E_0$  is very small.<sup>9</sup> We have measured the CuPt-type order birefringence in  $\text{Al}_x\text{Ga}_{1-x}\text{InP}$  as a function of the degree of ordering  $\eta$ , and will report on these results in a follow-up manuscript.<sup>25</sup> Very small birefringence is found and, except for the redshift of the fundamental gap transition energy  $E_0$ , there is practically no change in the refractive index values between slightly ordered or highly ordered samples. It therefore seems unlikely that the discrepancies between the CP-structure parameters and dielectric function spectra for  $\text{Al}_x\text{Ga}_{1-x}\text{InP}$  reported so far in the literature are due to CuPt-type ordering effects alone. We suppose that different approaches for experiment and analysis are mainly responsible for the different optical functions spectra shown in Fig. 7.

## V. CONCLUSIONS

The dielectric function  $\epsilon(E,x)$ , and the CP parameters for  $\text{Al}_x\text{Ga}_{1-x}\text{InP}$  are reported over the full range of compo-

sition  $x$  using spectroscopic ellipsometry at variable angle-of-incidence (VASE). Samples were chosen that revealed low-intensity, or no additional superlattice diffraction spots within their selected area diffraction patterns from transmission electron microscopy investigations. The order-induced birefringence near the fundamental-gap transition was measured and found to be negligible throughout. A parameterization is provided which allows immediate calculation of the  $\text{Al}_x\text{Ga}_{1-x}\text{InP}$  dielectric function for any composition  $0 \leq x \leq 1$ . The model provides spectral coverage from 0.75 to 5 eV, and allows excellent reproduction of  $\epsilon(E, x)$ . In particular, the MDF yields physically meaningful index of refraction ( $n$ ) and extinction ( $k$ ) coefficients near and below the fundamental-gap transition. The line shape model is based on the one-electron interband-transition approach as used by Kato *et al.*, Adachi *et al.*, and Ozaki *et al.*, but includes Gaussian-like broadening functions as suggested recently by Rakić and Majewski, and complex amplitudes for both the excitonic contribution to the  $E_1$  CP structure, and for the  $E_2$  CP term. The dielectric functions obtained here are KK consistent within the experimental error bars, whereas the individual contributions to the model dielectric function may not fully satisfy the KK requirement. Results have been compared with those obtained by previous authors, and difference are attributed to different approaches used for experiment and analysis, rather than to ordering related phenomena.

Note finally that the excitonic expression for the dielectric function of Holden *et al.*,<sup>40</sup> which is based on the more exact theoretical work of Elliott,<sup>41</sup> allows for reduction of excitonic and critical-point parameters. This approach suffers from unrealistic absorption below the fundamental gap as well. It may therefore be interesting to incorporate the Gaussian-like broadening into the Holden expression.

## ACKNOWLEDGMENTS

This work is supported by the Deutsche Forschungsgemeinschaft under Grant No. Rh 28-1/12. Financial support during part of this study was also provided by the Center for Microelectronic and Optical Materials Research and the National Science Foundation Contract No. DMI/9761473 to the University of Nebraska.

## APPENDIX: MODEL DIELECTRIC FUNCTION

Here we list all contributions to the MDF employed in this work. A detailed introduction to the framework of Adachi's critical-point MDF can be found in Ref. 12. Refer also to Rakić and Majewski (Ref. 13). Note that the Gaussian-like broadening dependence is applied to the excitonic contribution at the  $E_1$  CP, and to the contribution at the  $E_2$  CP only. Note further that all parameters on the right side of all equations below are positive and real valued except for  $i \equiv \sqrt{-1}$ , and the photon energy is  $E = \hbar\omega$ .

The  $E_0$  transition is a three-dimensional (3D)- $M_0$  CP. The contribution of the  $E_0$  CP structure to  $\epsilon(E)$  is<sup>12,42</sup>

$$\epsilon^{(0)}(E) = A_0 E_0^{-1.5} \{ \chi_0^{-2} [2 - (1 + \chi_0)^{0.5} - (1 - \chi_0)^{0.5}] \} \quad (\text{A1})$$

with  $\chi_j = (E + i\Gamma_j)/E_j$  [ $j=0, 1$  for Eqs. (A1), (A2), respectively].  $A_0$ ,  $E_0$ , and  $\Gamma_0$  are, respectively, amplitude, transition energy, and broadening parameter of the  $E_0$  CP structure.

The  $E_1$  transition is of the 3D- $M_1$  type. Because the  $M_1$ -CP longitudinal effective mass is much larger than the transverse effective mass, this CP is usually treated as a two-dimensional (2D)  $M_0$  CP.<sup>12</sup> The contribution of the  $E_1$  CP structure to  $\epsilon(E)$  is then given by

$$\epsilon^{(1)} = -A_1 \chi_1^{-2} \ln(1 - \chi_1^2). \quad (\text{A2})$$

$A_1$ ,  $E_1$ , and  $\Gamma_1$  are, respectively, amplitude, transition energy, and broadening parameter of the  $E_1$  CP structure. Contributions to  $\epsilon(E)$  due to ground-state Wannier-type 2D excitons are considered at the  $E_1$  CP structure. The exciton-induced dielectric susceptibility is approximated by a single damped Lorentzian (DL) line shape with complex amplitude, and energy-dependent broadening term<sup>8,13</sup>

$$\epsilon^{(1x)} = \frac{A_{1x} \exp(ip_{1x})}{E_1 - E - i\Gamma_{1x} \exp(-s_{1x}[E_1 - E]^2)}. \quad (\text{A3})$$

$A_{1x}$ , and  $p_{1x}$  are, respectively, amplitude and phase of the complex magnitude of the excitonic contribution.  $\Gamma_{1x}$  and  $s_{1x}$  are, respectively, amplitude and distribution parameter of the energy-dependent broadening term.

The  $E_2$  CP structure is characterized by a DHO with complex amplitude ( $A_2, p_2$ ) and energy-dependent broadening term ( $\Gamma_2, s_2$ )

$$\begin{aligned} \epsilon^{(2)} &= \frac{A_2 \exp(ip_2)}{1 - (E/E_2)^2 - i(E/E_2)(\Gamma_2/E_2) \exp(-s_2[E - E_2]^2)}. \end{aligned} \quad (\text{A4})$$

<sup>1</sup>G. B. Stringfellow, MRS Bull. **22**, 27 (1997).

<sup>2</sup>D. P. Bour, in *Quantum Well Lasers*, edited by P. S. Zory, Jr. (Academic, Boston, 1993).

<sup>3</sup>A. Zunger, MRS Bull. **22**, 20 (1997), and references therein.

<sup>4</sup>S.-H. Wei and A. Zunger, Phys. Rev. B **57**, 8983 (1998).

<sup>5</sup>S.-H. Wei, A. Franceschetti, and A. Zunger, Phys. Rev. B **51**, 13097 (1995).

<sup>6</sup>F. Alsina, M. Garriga, M. I. Alonso, J. Pascual, C. Geng, P. Ernst, and F. Scholz, Cryst. Res. Technol. **31**, 205 (1996).

<sup>7</sup>P. Y. Yu and M. Cardona, *Fundamentals of Semiconductors* (Springer, Berlin, 1995).

<sup>8</sup>H. Kato, S. Adachi, H. Nakanishi, and K. Ohtsuka, Jpn. J. Appl. Phys., Part 1 **33**, 186 (1994).

<sup>9</sup>R. Wirth, A. Moritz, C. Geng, F. Scholz, and A. Hangleiter, Phys. Rev. B **55**, 1730 (1997).

<sup>10</sup>M. Schubert, B. Rheinländer, E. Franke, I. Pietzonka, J. Skriniarova, and V. Gottschalch, Phys. Rev. B **54**, 17616 (1996).

<sup>11</sup>S. Adachi, *Physical Properties of III-V Semiconductor Compounds* (Wiley-Interscience, New York, 1992).

<sup>12</sup>S. Adachi, T. Kimura, and N. Suzuki, J. Appl. Phys. **74**, 3435 (1993).

<sup>13</sup>A. D. Rakić and M. L. Majewski, J. Appl. Phys. **80**, 5909 (1996).

<sup>14</sup>H. Lee, M. V. Klein, D. E. Aspnes, C. P. Kuo, M. Peanasky, and M. G. Craford, J. Appl. Phys. **73**, 400 (1993).

<sup>15</sup>M. Cardona, *Modulation Spectroscopy*, Suppl. 11 of *Solid State Physics* (Academic, New York, 1969).

<sup>16</sup>D. E. Aspnes, *Handbook on Semiconductors* (North-Holland, Amsterdam, 1980), Vol. 2, p. 109.

<sup>17</sup>H. Lee, M. V. Klein, J. M. Olson, and K. C. Hsieh, Phys. Rev. B **53**, 4015 (1996).

<sup>18</sup>H. Lee, D. Biswas, M. V. Klein, H. Morkoç, D. E. Aspnes, B. D. Choe, J.

- Kim, and C. O. Griffiths, J. Appl. Phys. **75**, 5040 (1994).
- <sup>19</sup>S. Adachi, S. Ozaki, M. Sato, and K. Ohtsuka, Jpn. J. Appl. Phys., Part 1 **35**, 537 (1996).
- <sup>20</sup>S. Ozaki, S. Adachi, M. Sato, and K. Ohtsuka, J. Appl. Phys. **79**, 493 (1996).
- <sup>21</sup>S. Adachi, H. Kato, A. Moki, and K. Ohtsuka, J. Appl. Phys. **75**, 478 (1994).
- <sup>22</sup>M. Moser, R. Winterhoff, C. Geng, I. Queisser, F. Scholz, and A. Dörnen, Appl. Phys. Lett. **64**, 235 (1994).
- <sup>23</sup>M. Kondow, H. Kakibayashi, and S. Minagawa, Phys. Rev. B **40**, 1159 (1989).
- <sup>24</sup>M. Schubert, B. Rheinländer, and V. Gottschalch, Solid State Commun. **95**, 723 (1995).
- <sup>25</sup>M. Schubert, T. Hoffman, B. Rheinländer, I. Pietzonka, T. Sass, and V. Gottschalch (unpublished).
- <sup>26</sup>R. M. A. Azzam and N. M. Bashara, *Ellipsometry and Polarized Light* (North-Holland, Amsterdam, 1977).
- <sup>27</sup>G. E. Jellison, Thin Solid Films **313,314**, 33 (1998), and references therein.
- <sup>28</sup>C. M. Herzinger, P. G. Snyder, B. Johs, and J. A. Woollam, J. Appl. Phys. **77**, 1715 (1995).
- <sup>29</sup>S. Zollner, Appl. Phys. Lett. **63**, 2523 (1993).
- <sup>30</sup>C. M. Herzinger, H. Yao, P. G. Snyder, F. G. Celii, Y.-C. Kao, B. Johs, and J. A. Woollam, J. Appl. Phys. **77**, 4677 (1995).
- <sup>31</sup>C. C. Kim, J. W. Garland, H. Abad, and P. M. Raccach, Phys. Rev. B **45**, 11749 (1992).
- <sup>32</sup>C. C. Kim, J. W. Garland, and P. M. Raccach, Phys. Rev. B **47**, 1876 (1993).
- <sup>33</sup>J. W. Garland, C. C. Kim, H. Abad, and P. M. Raccach, Phys. Rev. B **41**, 7602 (1990).
- <sup>34</sup>M. C. DeLong, D. J. Mowbray, R. A. Hogg, M. S. Skolnick, J. E. Williams, K. Meehan, S. R. Kurtz, J. M. Olson, R. P. Schneider, M. C. Wu, and M. Hopkinson, Appl. Phys. Lett. **66**, 3185 (1995).
- <sup>35</sup>M. Schubert, V. Gottschalch, C. M. Herzinger, H. Yao, P. G. Snyder, and J. A. Woollam, J. Appl. Phys. **77**, 3416 (1995).
- <sup>36</sup>*Guide to Using WVASE32* (Woollam, Lincoln, NE, 1995), pp. 216, 217.
- <sup>37</sup>F. Alsina, M. Garriga, M. I. Alonso, S. Tortosa, J. Pascual, C. Geng, F. Scholz, and R. W. Glew, Solid State Commun. **101**, 757 (1997).
- <sup>38</sup>J. S. Luo, J. M. Olson, S. R. Kurtz, D. J. Arendt, K. A. Bertness, M. E. Raikh, and E. V. Tsiper, Phys. Rev. B **51**, 7603 (1995).
- <sup>39</sup>J. S. Luo, J. M. Olson, Y. Zhang, and A. Mascarenhas, Phys. Rev. B **55**, 16385 (1997).
- <sup>40</sup>T. Holden, P. Ram, F. H. Pollak, J. L. Freeouf, B. X. Yang, and M. C. Tamargo, Phys. Rev. B **56**, 4037 (1997).
- <sup>41</sup>R. J. Elliott, Phys. Rev. **108**, 1384 (1957).
- <sup>42</sup>C. W. Higginbotham, M. Cardona, and F. Pollak, Phys. Rev. **184**, 821 (1969).